Thermal Stability of Magnetic States in Circular Thin-Film Nanomagnets with Large Perpendicular Magnetic Anisotropy

Gabriel D. Chaves-O'Flynn,[1] Georg Wolf,[1,*] Jonathan Z. Sun,[2] and Andrew D. Kent[1]

[1]*Department of Physics, New York University, New York, New York 10003, USA*
[2]*IBM T. J. Watson Research Center, Yorktown Heights, New York 10598, USA*

(Received 15 May 2015; revised manuscript received 8 July 2015; published 18 August 2015)

The scaling of the energy barrier to magnetization reversal in thin-film nanomagnets with perpendicular magnetization as a function of their lateral size is of great current interest for high-density magnetic random-access memory devices. Here we determine the micromagnetic states that set the energy barrier to thermally activated magnetization reversal of circular thin-film nanomagnets with large perpendicular magnetic anisotropy. We find a critical length in the problem that is set by the exchange and effective perpendicular magnetic anisotropy energies, with the latter including the size dependence of the demagnetization energy. For diameters smaller than this critical length, the reversal occurs by nearly coherent magnetization rotation and the energy barrier scales with the square of the diameter normalized to the critical length (for fixed film thickness), while for larger diameters, the transition state has a domain wall, and the energy barrier depends linearly on the normalized diameter. Simple analytic expressions are derived for these two limiting cases and verified using full micromagnetic simulations with the string method. Further, the effect of an applied field is considered and shown to lead to a plateau in the energy barrier versus diameter dependence at large diameters.

DOI: 10.1103/PhysRevApplied.4.024010

I. INTRODUCTION

Nanomagnets with bistable states are being explored for use in magnetic random-access memories (MRAM). Data loss is associated with relatively rare thermally activated transitions between magnetic states and is typically modeled with methods from statistical mechanics [1,2]. The rate of data loss is well approximated by an Arrhenius law $\Gamma = \Gamma_0 \exp(-U/k_BT)$, where U is the energy barrier to magnetization reversal, k_BT is Boltzmann's constant times the temperature, and Γ_0 is an attempt frequency set by a natural time scale of the system (typically, approximately 10^9 Hz). One major challenge in creating higher-density magnetic memory chips is maintaining a large $U/(k_BT)$ to ensure long-term data retention.

Recent developments in thin-film materials with large perpendicular magnetic anisotropy provide a path to achieving that goal [3–6]. Their anisotropy is associated with magnetocrystalline interface or bulk magnetic anisotropy [7–9]. As such, elements can be in the shape of a thin disk with their magnetization oriented perpendicularly to the plane of the disk. This allows denser packing of MRAM cells, since magnetic dipole interactions between neighboring magnetic elements is reduced in comparison to those of in-plane magnetized elements. However, the scaling of an element's energy barrier with the disk diameter remains a key issue. A macrospin model, where the magnetization is treated as uniform, predicts a quadratic increase of the energy barrier with the disk diameter.

However, experimental results from field-driven switching as well as spin-transfer torque-driven switching experiments in variable-diameter magnetic tunnel-junction devices with fixed layer thickness do not show the expected behavior. Reference [10] reports an almost linear dependence of the energy barrier on the device diameter. Reference [11] presents a quadratic scaling of the energy barrier below a distinct device diameter. Moreover, both studies show saturation of the energy barrier for large diameters.

A starting point to understand the thermally activated reversal is a macrospin model [12], where the energy density of an elliptically shaped magnetic element is given by

$$E = \frac{\mu_0 M_s^2}{2}\mathbf{m}\cdot\mathbf{N}\cdot\mathbf{m} - K_p m_z^2 - \mu_0 M_s \mathbf{m}\cdot\mathbf{H}_{\text{ext}}, \qquad (1)$$

where M_s is the saturation magnetization, $\mathbf{m}$ is a unit vector in the direction of magnetization, and m_z is its z component. $\mathbf{N}$ is the demagnetization tensor of the structure, K_p is the intrinsic perpendicular anisotropy energy density (energy per unit volume) of the material, and $\mathbf{H}_{\text{ext}}$ is an externally applied magnetic field. The energy barrier is defined as the difference between the metastable energy minima and the lowest-energy saddle state, also known as the transition state. Approximating the thin disk as an ellipsoid, the demagnetizing tensor is diagonal with trace 1 ($N_{xx} + N_{yy} + N_{zz} = 1$). Because of the cylindrical symmetry, the in-plane components of the tensor are equal ($N_{xx} = N_{yy}$), and the demagnetizing energy density can

*Corresponding author.
gw42@nyu.edu

be reduced to an expression that depends only on N_{zz}, the demagnetizing factor in the direction perpendicular to the film plane,

$$U = [K_p - \mu_0 M_s^2(3N_{zz} - 1)/4]\frac{\pi}{4}d^2 t. \quad (2)$$

Thus, in this model of coherent (macrospin) magnetization reversal, the energy barrier should depend mainly on the element area (or, equivalently, its volume) with corrections due to changes in the demagnetization factor with area.

However, this simple macrospin is a poor description of thermally activated reversal processes because the elements studied experimentally are typically larger than characteristic magnetic lengths. One length scale is set by the width of a domain wall, which is related to the ratio of the exchange constant A (in J/m) [13] to the effective anisotropy per unit volume K_{eff}, $\lambda_{\text{DW}} = \sqrt{A/K_{\text{eff}}}$. We assume the effective anisotropy per unit volume $K_{\text{eff}} = K_p - \mu_0 M_s^2(3N_{zz} - 1)/4$, consisting of a contribution from the intrinsic anisotropy K_p and a counteracting demagnetizing term, discussed further below. We treat the demagnetizing energy as we did in the macrospin model, which is a good approximation for a nonuniform magnetization configuration of a domain wall as long as the magnetic elements are much larger than the domain-wall width. The energy density per unit length for a domain wall is given then by [14]

$$E = 4\sqrt{AK_{\text{eff}}}t. \quad (3)$$

The energy associated with creating a domain wall that bisects a magnetic element is, thus, given by

$$U = 4\sqrt{AK_{\text{eff}}}dt \quad (4)$$

and depends linearly on the diameter of the element.

In a prior modeling study by some of the authors, a linear dependence of the energy barrier on diameter over a large range of sample sizes was found [15]. It also indicates that the transition state has a domain wall, which in zero applied field, bisects the element. A puzzling result is that even at seemingly small sample diameters, the energy barrier does not depend on the area, but it continues to be proportional to the disk diameter. In contrast to this previous work, we determine the length scale at which there is a crossover between uniform and nonuniform thermally activated magnetization reversal and a corresponding change in the relationship between the energy barrier and element size. We also show the effect of applied fields on the transition state and energy barrier and find a saturation of the energy barrier at large element sizes. Analytic results are derived that can guide experimental analysis and magnetic device design.

II. RESULTS

A. Analytic model

The basic physics can be seen from Eqs. (2) and (4). For a given material system, there is a critical diameter d_c where the domain-wall energy becomes less than the energy barrier for the coherent reversal. The critical diameter depends on the square root of the ratio of the exchange constant and the effective anisotropy,

$$d_c = \frac{16}{\pi}\sqrt{\frac{A}{K_{\text{eff}}(d)}}. \quad (5)$$

Since $K_{\text{eff}}(d)$ depends on the diameter, this expression must be evaluated for each element diameter using the appropriate demagnetizing factor $N_{zz}(d)$. Figure 1(a) shows the demagnetization factor $(3N_{zz} - 1)/2$ of a disk as a function of d/t. We choose to compute the demagnetizing energy numerically by saturating the sample along its principal axes and treat the result as the equivalent demagnetizing tensor elements as described in Ref. [16]. It is clear that the demagnetizing energy is significantly reduced as the diameter is decreased, even for aspect ratios

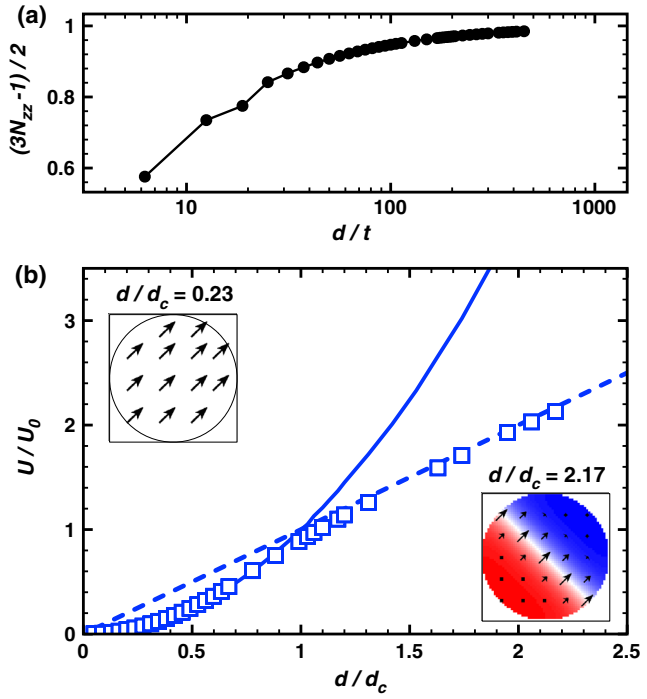

FIG. 1. (a) Demagnetizing coefficient as a function of the ratio of disk diameter d to thickness t. (b) Rescaled energy barrier U/U_0 for macrospin reversal (solid line) and for a domain state (dashed line) as a function of the normalized diameter d/d_c. The blue open squares represent energy barriers obtained from micromagnetic simulations using the string method. The insets show the micromagnetic configuration of the transition states for the coherent reversal $d/d_c = 0.23$ and domain-wall $d/d_c = 2.17$ cases.

as large as approximately 50. For typical film thicknesses between 1 and 2 nm, this aspect ratio corresponds to elements that are less than 50 nm in diameter, which are in the size range that are of great importance technologically (see, for example, Ref. [3]). Thus, this correction factor due to the finite-size disk aspect ratio needs to be considered when investigating the thermal stability. Ferromagnetic resonance experiments on magnetic tunnel junctions show a similar trend of the effective anisotropy decreasing with increasing device diameter [17].

In Ref. [15], material parameters for Co/Ni multilayers were used ($A = 8.3\,\mathrm{pJ/m}$, $M_s = 713\,\mathrm{kA/m}$, $K_p = 403\,\mathrm{kJ/m^3}$, and $t = 1.6$ nm), resulting in a critical diameter of $d_c \approx 40$ nm. The number of elements smaller than this was quite limited in that study, so the crossover between coherent rotation and domain-wall reversal could not be observed clearly.

The macrospin U_{MS} [Eq. (2)] and domain-wall U_{DW} [Eq. (4)] energy barriers can be rewritten in terms of d_c to show that their characteristic scale is a product of the exchange constant and film thickness At. We denote U_0,

$$U_0 = \frac{64}{\pi} At, \tag{6}$$

$$\frac{U_{\mathrm{MS}}}{U_0} = \left(\frac{d}{d_c}\right)^2, \tag{7}$$

$$\frac{U_{\mathrm{DW}}}{U_0} = \frac{d}{d_c}. \tag{8}$$

For this reason, we can choose a different set of material parameters that allow us to study this crossover more conveniently to avoid discretization issues in micromagnetic modeling that occur for very small element sizes. We take $M_s = 300$ kA/m, $A = 83.0$ pJ/m, $K_p = 83.6$ kJ/m^3, and $t = 1.6$ nm to give a critical diameter of $d_c \approx 275$ nm. The material parameters are considered to be constant throughout the sample volume, since spatial variations are a rather complex topic and beyond the scope of this study.

Figure 1(b) shows the rescaled energy barrier as a function of the ratio d/d_c for the set of material parameters chosen here. Using the rescaled expression, the curves for both material parameters fall on top of each other, which demonstrates that we have identified the relevant length and energy scales in this problem.

B. Micromagnetic modeling

In order to confirm this simple model's predictions, we also perform string method calculations [18], a minimal energy path method, which evolved in the OOMMF [19] framework without the precessional term, as described in Ref. [15]. The parametrized string consists of a set of micromagnetic configurations connecting the two stable configurations of the disk. The micromagnetic state with highest energy in the converged string corresponds to the transition state, and the difference in energy with respect to the equilibrium state is the energy barrier. The open blue squares in Fig. 1(b) show the energy barriers obtained by this method for a wide range of element diameters. The insets in Fig. 1(b) also shows the micromagnetic transition states for a disk with d/d_c ratio 0.23 (60 nm) and 2.17 (600 nm) representing the two different reversal regimes. The $d/d_c = 0.23$ disk reverses through a nearly coherent process, while in the $d/d_c = 2.17$ disk, a domain wall that bisects the element is the lowest-energy transition state. The micromagnetic results agree with the predictions of the macrospin model up to the critical diameter (d_c) where the domain-wall transition state becomes lower in energy; above d_c, the simulation results follow the domain-wall energy barrier. This *quantitative* agreement can be achieved only by using the demagnetization factor $N_{zz}(d)$ from Fig. 1 in Eq. (2). The energy barriers found in the micromagnetic simulation, which captures the full nonlocal nature of the dipole-dipole interactions, does not deviate from those predicted by the macrospin model nor does it deviate from those for a simple domain-wall model in their respective regimes. This result demonstrates that a thin-film nanomagnet in the shape of a circle can be treated within a model where the demagnetizing field is considered in a spatially averaged way, i.e., with only a single value N_{zz}, that gives the appropriate demagnetization energy for a uniformly magnetized element. However, as already noted, this value is a function of the sample diameter, as shown in Fig. 1(a).

C. Effect of applied fields

In experimental studies, it is also noted that fringe fields from a proximal magnetic reference layer (e.g., in a magnetic tunnel junction or spin valve) might alter the energy barrier [11,20]. Thus, in addition to this zero-field case, we also study the dependence of the energy barrier on a perpendicularly applied field. In the macrospin limit, the energy barrier still scales with the volume, only the prefactor (i.e., U_0) is altered by the field. However, in the domain-wall transition-state limit, the situation is more complex. In addition to the domain-wall energy, there is now a reduction of the energy barrier due to the Zeeman energy from the reversed subvolume of the magnet which has to be considered,

$$U = -2\mu_0 M_s H_{\mathrm{ext}} \Omega t + 4\sqrt{A K_{\mathrm{eff}}}\,\Lambda t, \tag{9}$$

where Ω is the area of the subvolume and Λ the length of the domain wall, which have the unit of a length and, thus, should be normalized to d_c,

$$\frac{U}{U_0} = -\frac{16}{\pi}\frac{H_{\mathrm{ext}}}{H_k}\frac{\Omega}{d_c^2} + \frac{\Lambda}{d_c}. \tag{10}$$

H_k is the effective anisotropy field, $H_k = 2K_{\text{eff}}/(\mu_0 M_s)$. The problem now becomes an optimization of the area of the subvolume versus its perimeter. The string method calculations [see Fig. 2(a)] reveal that the transition state at larger diameters form a domain state with a curved wall, where the area and length of the wall depend on the diameter. It is plausible that the shape of the reversed section is circular. In a simple model the reversed area is enclosed by the overlap of two intersecting circles of the diameters d and d_s and opening angles ϕ and ϕ_s [see Fig. 2(b)]. This model assumes that the domain wall forms a 90° angle with the edge of the element, which minimizes the wall length. This 90° angle constrains the opening angles and the diameters to be

$$\phi + \phi_s = \pi/2, \qquad \frac{d_s^2}{d^2} = \tan(\phi). \tag{11}$$

Under these assumptions, the total area Ω and the length of the wall Λ can be written in terms of the element diameter d and the opening angle ϕ,

$$\Omega = \frac{\phi}{4}d^2 - \frac{1}{8}d^2\sin(2\phi) - \frac{\pi/2-\phi}{4}d^2\tan^2(\phi) + \frac{1}{8}d^2\tan^2(\phi)\sin(2\phi), \tag{12}$$

$$\Lambda = d\left(\frac{\pi}{2} - \phi\right)\tan(\phi). \tag{13}$$

The energy is a nontrivial function of ϕ with a maximum that represents the energy barrier

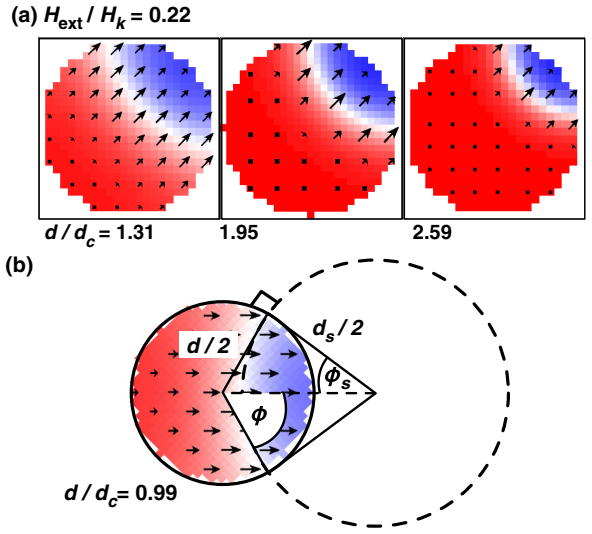

FIG. 2. (a) Transition states for different diameters larger than the critical diameter in an applied field of $0.22H_k$ (40 mT). (b) Geometry of the domain-wall transition state in an applied field. Reversed area Ω is given by the intersection of two circles, one the set by the diameter of the element d and the other by the diameter of the reversed subvolume d_s, with opening angles ϕ and ϕ_s.

$$\frac{U}{U_0} = \frac{d}{d_c}\left(\frac{\pi}{2} - \phi_{\max}\right)\tan(\phi_{\max}) - \frac{H_{\text{ext}}}{H_k}\left(\frac{d}{d_c}\right)^2\left[\frac{\phi_{\max}}{4} - \frac{1}{8}\sin(2\phi_{\max}) - \frac{\pi/2-\phi_{\max}}{4}\tan^2(\phi_{\max}) + \frac{1}{8}\tan^2(\phi_{\max})\sin(2\phi_{\max})\right]. \tag{14}$$

We choose to find the maximum numerically, since deriving an analytical expression for $\phi_{\max}$ is not possible. Figure 3 shows the combined results of the string method and the analytic models. The energy barriers obtained from the string method (dots) for small diameters follow the quadratic dependency of the macrospin and are in good agreement with the solutions of the domain-wall model (dashed lines) in the case of the larger diameters. In general, larger fields lead to less change in the energy barrier as the diameter increases. In the limit of a very large ratio of d/d_c, the reversed area becomes a semicircle and the energy barrier saturates. The saturation energy barrier U_{sat} and the saturation diameter d_{sat} are given by the ratio of the applied field to the anisotropy field,

$$\frac{U_{\text{sat}}}{U_0} = \frac{\pi^2}{32}\frac{H_k}{H_{\text{ext}}}, \qquad \frac{d_{\text{sat}}}{d_c} = \frac{\pi}{8}\frac{H_k}{H_{\text{ext}}}. \tag{15}$$

This field dependence of the energy barrier might explain the experimentally observed saturation of the energy barrier for larger diameters. The model shows a plateau in the energy barrier at a diameter only twice as big as the critical diameter for an external field of 20% of the anisotropy field. It is usually assumed that the stray field from the

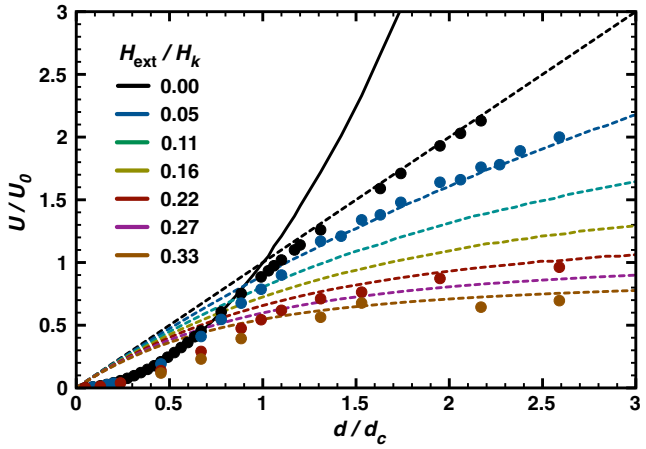

FIG. 3. Energy barriers normalized to U_0 calculated by the domain-wall model Eq. (14) (dashed lines) and obtained with the string method (solid points) for different applied fields and disk diameters. The black solid line corresponds to the macrospin model without applied field.

reference layer is much less than the anisotropy field of the free layer. We note that the model prediction is for a uniform field in the perpendicular direction, while in real devices, the stray field has a nonuniform distribution across the device and in-plane components, which might enhance this effect. Also, defects in the structure can function as nucleation centers for a domain wall, and are not considered in our model.

III. DISCUSSION

This study determines the energy barrier for thermally activated magnetization reversal, which gives the lifetime for data retention of such a magnetic element in a storage device and, thus, the device's thermal stability. From Eq. (5), it is clear that as K_{eff} is increased to increase the stability of smaller elements, the critical diameter also decreases, and a domain-wall state can become the lowest-energy saddle state further reducing the stability. This reduction in the thermal stability can be counteracted only by increasing the exchange energy. It will, thus, be of greater importance when scaling to smaller dimensions to not only increase the perpendicular magnetic anisotropy of magnetic memory elements but also increase their exchange energy.

Furthermore, in a macrospin model for spin-transfer torque-driven reversal, the critical current density is directly proportional to the anisotropy field. Thus, the critical current should show a similar dependence on the device size as the energy barrier for sample diameters less than the critical diameter d_c. For larger diameters, it is presently not clear if the energy barrier and critical current will scale in the same way with the sample diameter. The experimental results reported in Ref. [10] show that the critical write current density is almost independent of the device area and, thus, appears not to be correlated to the energy barrier; this suggests that the critical current density continues to be proportional to the anisotropy field while the energy barrier does not. Recent modeling of the spin-transfer torque-switching dynamics in perpendicularly magnetized disks reveals that a dynamic instability leads to an incoherent reversal [21]. The instantaneous spatial profile of this instability shows a domainlike state, which can reduce the effective energy barrier during reversal, as we show here. This topic deserves further study, particularly how the spin-current-induced instabilities reported in Ref. [21] vary with disk diameter in the regimes identified here.

IV. SUMMARY

In summary, we demonstrate that the scaling of the energy barrier of a circularly shaped thin-film nanomagnet with perpendicular anisotropy depends strongly on the ratio between exchange constant A and the effective anisotropy K_{eff}. Only large exchange and relatively small effective perpendicular anisotropy will lead to the quadratic scaling of the energy barrier on normalized diameter d/d_c. The energy barriers determined with the string method and micromagnetics confirm that the analytical macrospin and domain-wall model describe the scaling when appropriate demagnetizing factors are used in the analytic model. Even in an applied field, there is an analytic expression for the geometrical configuration of the magnetization that describes the transition states, and, thus, a prediction of the energy barrier can be made without extensive numerical calculations. We also observe a plateau of the energy barrier for larger fields and large diameters of the disk, at a value which depends on the ratio of the applied field to the anisotropy field.

ACKNOWLEDGMENTS

This research is supported by Grant No. NSF-DMR-1309202 and in part by Spin Transfer Technologies Inc. and the Nanoelectronics Research Initiative through the Institute for Nanoelectronics Discovery and Exploration.

[1] W. F. Brown, Thermal fluctuations of a single-domain particle, Phys. Rev. **130**, 1677 (1963).
[2] W. T. Coffey and Y. P. Kalmykov, Thermal fluctuations of magnetic nanoparticles: Fifty years after Brown, J. Appl. Phys. **112**, 121301 (2012).
[3] A. D. Kent and D. C. Worledge, A new spin on magnetic memories, Nat. Nanotechnol. **10**, 187 (2015).
[4] S. Mangin, D. Ravelosona, J. A Katine, M. Carey, B. D. Terris, and E. E. Fullerton, Current-induced magnetization reversal in nanopillars with perpendicular anisotropy, Nat. Mater. **5**, 210 (2006).
[5] S. Ikeda, K. Miura, H. Yamamoto, K. Mizunuma, H. D. Gan, M. Endo, S. Kanai, J. Hayakawa, F. Matsukura, and H. Ohno, A perpendicular-anisotropy CoFeB-MgO magnetic tunnel junction, Nat. Mater. **9**, 721 (2010).
[6] D. C. Worledge, G. Hu, D. W. Abraham, J. Z. Sun, P. L. Trouilloud, J. Nowak, S. Brown, M. C. Gaidis, E. J. O'Sullivan, and R. P. Robertazzi, Spin torque switching of perpendicular Ta-CoFeB-MgO-based magnetic tunnel junctions, Appl. Phys. Lett. **98**, 022501 (2011).
[7] G. H. O. Daalderop, P. J. Kelly, and F. J. A. den Broeder, Prediction and Confirmation of Perpendicular Magnetic Anisotropy in Co/Ni Multilayers, Phys. Rev. Lett. **68**, 682 (1992).
[8] J. M. Shaw, H. T. Nembach, and T. J. Silva, Measurement of orbital asymmetry and strain in $Co_{90}Fe_{10}$/Ni multilayers and alloys: Origins of perpendicular anisotropy, Phys. Rev. B **87**, 054416 (2013).
[9] S. Mizukami, F. Wu, A. Sakuma, J. Walowski, D. Watanabe, T. Kubota, X. Zhang, H. Naganuma, M. Oogane, Y. Ando, and T. Miyazaki, Long-Lived Ultrafast Spin Precession in Manganese Alloys Films with a Large Perpendicular Magnetic Anisotropy, Phys. Rev. Lett. **106**, 117201 (2011).
[10] J. Z. Sun *et al.*, Spin-torque switching efficiency in CoFeB-MgO based tunnel junctions, Phys. Rev. B **88**, 104426 (2013).

[11] H. Sato, E. C. I. Enobio, M. Yamanouchi, S. Ikeda, S. Fukami, S. Kanai, F. Matsukura, and H. Ohno, Properties of magnetic tunnel junctions with a MgO/CoFeB/Ta/CoFeB/MgO recording structure down to junction diameter of 11 nm, Appl. Phys. Lett. **105**, 062403 (2014).

[12] E. C. Stoner and E. P. Wohlfarth, A mechanism of magnetic hysteresis in heterogeneous alloy, Phil. Trans. R. Soc. A **240**, 599 (1948).

[13] A. Aharoni, *Introduction to the Theory of Ferromagnetism*, 2nd ed. (Oxford University Press, New York, 2000).

[14] A. Hubert and R. Schäfer, *Magnetic Domains*, 2nd ed. (Springer-Verlag, Berlin, 1998).

[15] G. D. Chaves-O'Flynn, E. Vanden-Eijnden, D. L. Stein, and A. D. Kent, Energy barriers to magnetization reversal in perpendicularly magnetized thin film nanomagnets, J. Appl. Phys. **113**, 023912 (2013).

[16] M. Beleggia, M. De Graef, and Y. T. Millev, The equivalent ellipsoid of a magnetized body, J. Phys. D **39**, 891 (2006).

[17] K. Mizunuma, M. Yamanouchi, H. Sato, S. Ikeda, S. Kanai, F. Matsukura, and H. Ohno, Size dependence of magnetic properties of nanoscale CoFeB-MgO magnetic tunnel junctions with perpendicular magnetic easy axis observed by ferromagnetic resonance, Appl. Phys. Express **6**, 063002 (2013).

[18] W. E, W. Ren, and E. Vanden-Eijnden, Simplified and improved string method for computing the minimum energy paths in barrier-crossing events, J. Chem. Phys. **126**, 164103 (2007).

[19] The Object Oriented MicroMagnetic Framework (OOMMF) project at ITL/NIST, 2011, http://math.nist.gov/oommf/.

[20] D. B. Gopman, D. Bedau, S. Mangin, C. H. Lambert, E. E. Fullerton, J. A. Katine, and A. D. Kent, Asymmetric switching behavior in perpendicularly magnetized spin-valve nanopillars due to the polarizer dipole field, Appl. Phys. Lett. **100**, 062404 (2012).

[21] K. Munira and P. B. Visscher, Calculation of energy-barrier lowering by incoherent switching in spin-transfer torque magnetoresistive random-access memory, J. Appl. Phys. **117**, 17B710 (2015).